Heliyon 6 (2020) e03185

Contents lists available at ScienceDirect

Heliyon

journal homepage: www.cell.com/heliyon

Research article

New thiazole, pyridine and pyrazole derivatives as antioxidant candidates: synthesis, DFT calculations and molecular docking study

Yassine Kaddouri [a], Farid Abrigach [a], El Bekaye Yousfi [b], Mohamed El Kodadi [a,c], Rachid Touzani [a,*]

[a] Laboratory of Applied Chemistry and Environment (LCAE), Faculty of Sciences, Mohamed First University, Oujda, Morocco
[b] Instituts Supérieurs des Professions Infirmières et Techniques de Santé (ISPITS), Hopital Al Farabi, Oujda, Morocco
[c] CRMEF Oriental, Centre Régional des Métiers de l'Education et de Formation Oujda, Morocco

ARTICLE INFO

Keywords:
Organic chemistry
Theoretical chemistry
Pharmaceutical chemistry
1,3-Thiazole
Pyridine
Phenol
DPPH
Antioxidant activity
DFT
Docking

ABSTRACT

Novel heterocyclic compounds containing pyrazole, thiazole and pyridine moieties were designed and prepared based on the condensation reaction between 1,3-thiazole or aminopyridine derivatives and 1H-pyrazole,3,5-dimethyl-1H-pyrazole or 1,2,4-triazole. Their structures were confirmed with FTIR, ^{1}H and ^{13}C NMR analyses. DPPH scavenging assay was used to evaluate their antioxidant potential. The ligand **4** showed the best antioxidant activity with an IC_{50} = 4.67 μg/mL, while IC_{50} values of the other compounds were found to be ranging from 20.56 to 45.32 μg/mL. DFT and molecular docking studies were performed in order to gain better insights and to understand the relationship between the structures of the studied compounds and their antioxidant activities. The results obtained revealed a good agreement between the experimental and the theoretical findings.

1. Introduction

Oxidative stress induced by the presence of free radicals which can damage cell membranes, membrane lipids and nucleic acids. This process has been noticed in the pathogen of aging and other diseases such as cancer, atherosclerosis, and Alzheimer's disease (Farbstein et al., 2010; Pietta, 2000). As a result, the elimination of free radicals and related species has attracted much attention in recent years. Heterocyclic compounds show best interests in this subject, such as 1,3-thiazole, which is one of the important five-membered rings containingnitrogen and sulfur as heteroatoms (Nayak and Gaonkar, 2019). It's a known scaffold as a potential pharmacophore in many biological activities (Abdel-sattar and El-naggar, 2017; Hussein and Turan, 2018; Lettre et al., 2010; Scarim et al., 2019; Varghese et al., 2016; Yadav and Senthilkumar, 2011). In addition, pyrazole, which is a five-membered heterocyclic ring containing two adjacent nitrogen, can be found in many industrial fields (Chauhan et al., 2011; Karrouchi et al., 2018; Khan et al., 2016; Yerragunta et al., 2014). The pyridine,a six-membered heterocyclic ring contains a only one nitrogen used for many applications (Carolina, 2008; Process et al., 2002). Based on a search made by Web of science database; from 1993 to 2018, the number of documents per year for these three heterocyclic moieties has known a remarkable increase as a represented in Figures 1, 2, and 3.

In the literature, there are many studies about antioxidant activity of heterocyclic compounds, and the closest ones are the N-((3,5-dimethyl-1H-pyrazol-1-yl)methyl)pyridin-4-amine derivatives (Abrigach et al., 2014a,b) which is represented in the Figure 4, where the compounds show good results of 27.51, 15.89, 28.11 and 57.12 mg/mL for $IC_{50}$of 1, 3, 8 and 10 respectively.

These results drive us firstly to prepare new heterocyclic compounds containing these cores, and then evaluate their antioxidant activity using DPPH scavenging method. Secondly, to investigate their molecular reactivity relationship based on DFT and molecular docking with the Urate oxidase.

The three-dimensional structure of the studied protein is Urate oxidase from aspergillus flavus complexed with its inhibitor oxonic acid (PDB: 1R4U) (Retailleau et al., 2004) shown in Figure 5, is an essential enzyme responsible for the first step in the degradation of uric acid to allantoin by formation of the intermediate (5-hydroxyisourate) and H_2O_2 as by-product (Figure 6). This enzyme demonstrated its activity to

* Corresponding author.
E-mail address: r.touzani@ump.ac.ma (R. Touzani).

https://doi.org/10.1016/j.heliyon.2020.e03185
Received 20 July 2019; Received in revised form 24 August 2019; Accepted 6 January 2020

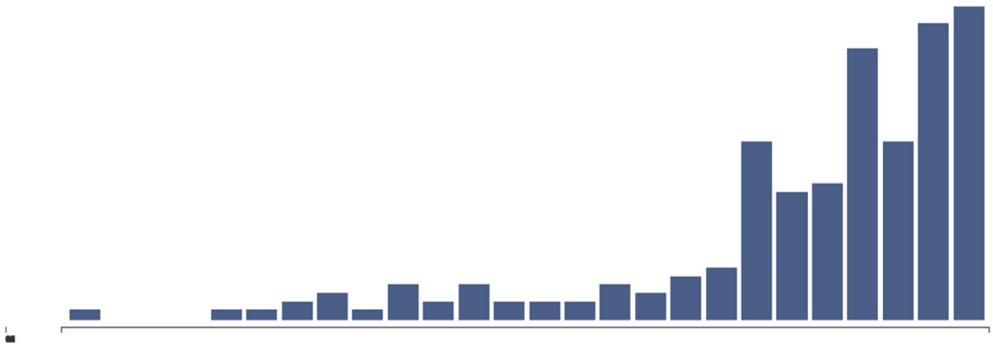

Figure 1. Citation report of "Thiazole and antioxidant" in web of science from 1993 to 2018.

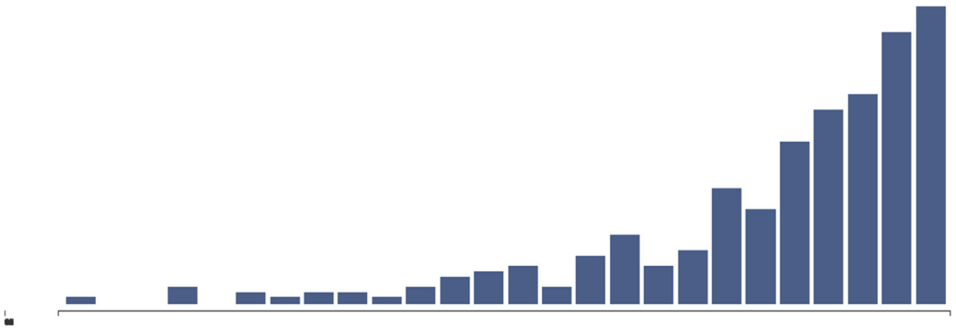

Figure 2. Citation report of "Pyrazole and antioxidant" in web science from 1993 to 2018.

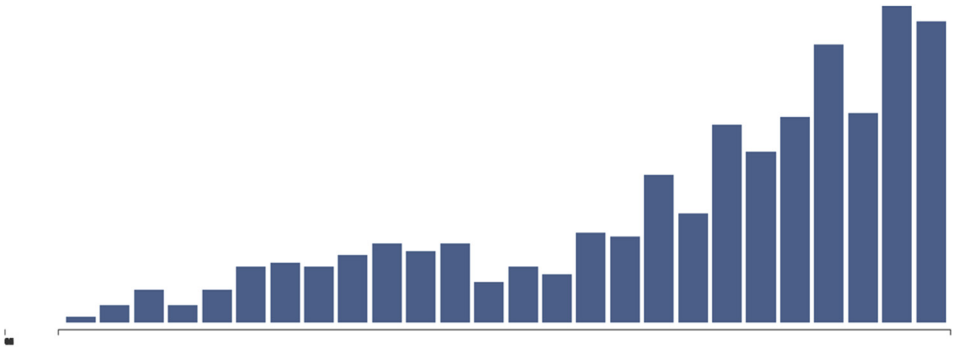

Figure 3. Citation report of "Pyridine and antioxidant" in web of science from 1993 to 2018.

oxidize the uric acid, and it described in the literature as one of the proteins docked to study theoretically the antioxidant activity (Retailleau et al., 2004; Tareq et al., 2019).

2. Materials and methods

2.1. General information

For the chemical analysis of the prepared ligands, several physico-chemical methods were used such as NMR by AVANCE 400 and 500 MHz of BRUKER to verify the structure of the product, using $CDCl_3$, CD_2Cl_2 and DMSO-d_6 as a solvent for ^1H NMR and ^{13}C NMR. The FTIR analyses were done by FTIR 8400S spectrophotometer recorded in KBr pellets.

2.2. Compounds synthesis

- **N,N-bis((1H-pyrazol-1-yl)methyl)thiazol-2-amine (1):**For this preparation, 1g of 2-aminothiazole (9.98 mmol) and 1.96g of (1H-pyrazol-1-yl)methanol (19.9mmol) were mixed together in acetonitrile under reflux for 4 h, and the solvent was evaporated then recrystallized in diethyl ether then filtrated to have the final product (2.58 g, 90%): **mp** 84–86 °C, **FTIR (KBr, cm^{-1}):** 3025 (C–H); 1560 (C=C); 1540 (C–C); 1386 (C–N); 1159 (C=N); 1050 (N–N); 754 (=C–H); 692 (C–S), **^1H NMR(CD_2Cl_2, 500MHz) δ ppm:** 7.79 (d, 2H, CH (5, Pyrazole), $J_{H\text{-}H} = 5$ Hz); 7.55 (d, 1H, CH–N, $J_{H\text{-}H} = 5$ Hz); 7.17 (d, 2H, CH (3, Pyrazole), $J_{H\text{-}H} = 5$ Hz); 6.62 (d, 1H, CH–S); 6.28 (t, 2H, CH (4, Pyrazole), $J_{H\text{-}H} = 5$ Hz); 5.56 (s, 4H, CH_2), **^{13}C NMR(CD_2Cl_2, 500MHz) δ ppm:** 167.75 (C–N); 139.80 (CH (3, Pyrazole)); 138.79 (CH–N); 129.53 (CH (5, Pyrazole)); 109.76 (CH–S); 105.42 (CH (4, Pyrazole)); 59.81 (CH_2).
- **N, N-bis((1H-pyrazol-1-yl)methyl)pyridin-4-amine(2):** For this preparation, 0.43g of 4-aminopyridine (4.55 mmol) and 0.89g of (1H-pyrazol-1-yl)methanol (9.07 mmol) were mixed together in acetonitrile under reflux for 4 h, and the solvent was evaporated then recrystallized in diethyl ether then filtrated to have the final product (0.67 g, 57%): **mp**68-70 °C; **FTIR (KBr, cm^{-1}):** 2372 (C–H); 1600 (C=C); 1564 (C–C); 1398 (C–N); 1306 (C=N); 1112 (N–N); 805 (=C–H), **^1H NMR(DMSO, 500MHz) δ ppm:** 8.10 (d, 2H, CH=N

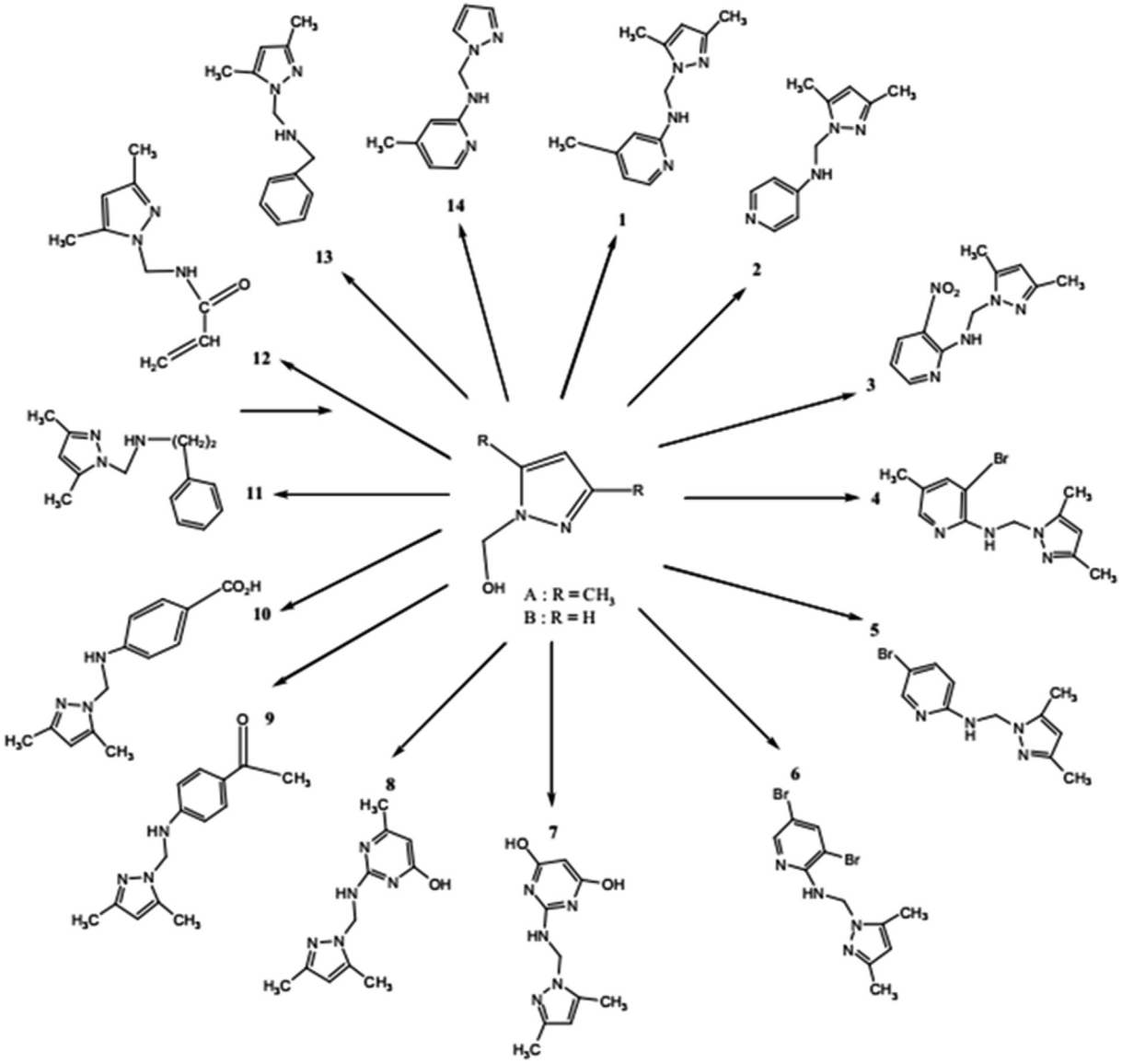

Figure 4. General reaction of the N-((3,5-dimethyl-1H-pyrazol-1-yl)methyl)pyridin-4-amine derivatives (Abrigach et al., 2014a,b).

(pyridine), J_{H-H} = 5 Hz); 7.79 (d, 2H, CH (5, pyrazole), J_{H-H} = 5 Hz); 7.52 (d, 2H, CH (3, pyrazole), J_{H-H} = 5 Hz); 6.78 (d, 2H, CH=C–N, J_{H-H} = 5 Hz); 6.26 (t, 2H, CH (4, Pyrazole), J_{H-H} = 5 Hz); 5.40 (s, 2H, CH_2), **^{13}C NMR(DMSO, 500MHz) δ ppm:** 152.89 (C–N); 150.02 (CH=N (pyridine)); 139.43 (CH (3, pyrazole)); 129.85 (CH (5, pyrazole)); 108.62 (CH=C–N); 106.10 (CH (4, Pyrazole)); 73.73 (CH_2).

- **N, N-bis((3,5-dimethyl-1H-pyrazol-1-yl)methyl)pyridin-4-amine(3):** For this preparation, 0.5g of 4-aminopyridine (5.31 mmol) and 1.34g of (3,5-dimethyl-1H-pyrazol-1-yl)methanol (11mmol) were mixed together in acetonitrile under reflux for 4 h, and the solvent was evaporated then recrystallized in diethyl ether then filtrated to have the final product (0.48 g, 29%): **mp** 100–102 °C, **FTIR (KBr, cm-1):** 2359 (C–H); 1648 (C=C); 1559 (C–C); 1454 (C–N); 1310 (C=N); 1071 (N–N); 807 (=C–H), **^{1}H NMR(CDCl$_3$, 500MHz) δ ppm:** 7.66 (d, 2H, C**H**=N (pyridine), J_{H-H} = 5 Hz); 7.24 (d, 2H, CH=C–N, J_{H-H} = 5 Hz); 6.24 (s, 2H, CH (4, Pyrazole)); 5.66 (s, 4H, CH_2); 2.34 (s, 6H, CH_3 (5, pyrazole)); 2.09 (s, 6H, CH_3 (3, pyrazole)), **^{13}C NMR(CDCl$_3$, 500MHz) δ ppm:** 167.73 (C–N (pyridine)); 156.11 (C=N); 140.41 (C–H (3, pyridine)); 138.13 (C–H (5, pyridine)); 113.78 (CH–CH=N); 105.50 (CH (Pyrazole)); 57.61 (CH_2); 14.02 (CH_3 (3, pyrazole)); 10.96 (CH_3 (5, pyrazole)).
- **N,N-bis((3,5-dimethyl-1H-pyrazol-1-yl)methyl)thiazol-2-amine(4)** (Kalanithi et al., 2015): For this preparation, 1.5g of 2-aminothiazole (0.0149 mol) and 3.78g of (3,5-dimethyl-1H-pyrazol-1-yl) methanol (0.0299 mol) were mixed together in acetonitrile under reflux for 4 h, and the solvent was evaporated then recrystallized in diethyl ether then filtrated to have the final product (3.58 g, 76%);**FTIR (KBr, cm^{-1}):** 3040 (C–H); 1558 (C=C); 1542 (C–C); 1320 (C–N); 1170 (C=N); 1030 (N–N); 742 (=C–H); 680 (C–S), **^{1}H NMR(DMSO, 400MHz) δ ppm:** 7.57 (d, 1H, CH–N (Thiazole), J_{H-H} = 5 Hz); 6.90 (d, 1H, CH–S (Thiazole), J_{H-H} = 5 Hz); 6.12 (s, 2H, CH (4, Pyrazole)); 5.59 (s, 4H, CH_2); 2.5 (s, 6H, CH_3 (5, pyrazole)); 2.16 (s, 6H, CH_3 (3, pyrazole)), **^{13}C NMR(DMSO, 400MHz) δ ppm:** 153.64 (C–N); 146.94 (C–CH_3 (3, pyridine)); 140.15 (C–CH_3 (5, pyridine)); 133.32 (CH–N (Thiazole)); 113.53 (CH–S (Thiazole)); 105.79 (CH (4, Pyrazole)); 61.32 (CH_2); 13.83 (CH_3 (3, pyrazole)); 10.29 (CH_3 (5, pyrazole)).
- **4-(bis((1H-pyrazol-1-yl)methyl)amino)phenol(5):** For this preparation, 0.9g of 4-aminophenol (8.24 mmol) and 2g of (1H-pyrazol-1-yl)methanol (20 mmol) were mixed together in acetonitrile under reflux for 4 h, and the solvent was evaporated then recrystallized in diethyl ether then filtrated to have the final product (1.79 g, 81%):

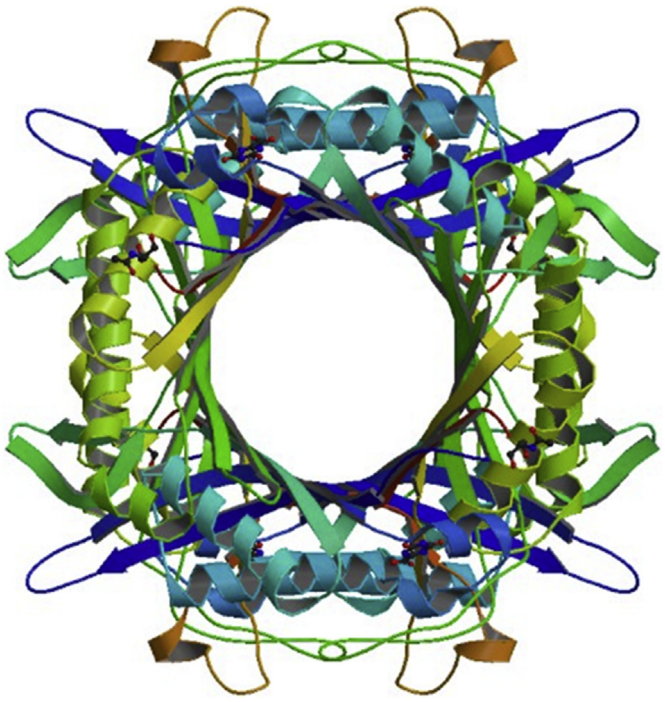

Figure 5. The three-dimensional structure of the urate oxidase from aspergillus flavus complexed with its inhibitor oxonic acid (PDB:1R4U).

mp 158–160 °C, **FTIR (KBr, cm^{-1}):** 3113 (O–H); 2300 (C–H); 1659 (C=C); 1509 (C–C); 1393 (C–N); 1183 (C=N); 1039 (N–N); 750 (=C–H), **^{1}H NMR(DMSO, 500MHz) δ ppm:** 8.75 (s, 1H, OH); 7.86 (d, 2H, CH (5, pyrazole), J_{H-H} = 5 Hz); 7.58 (d, 2H, CH (3, pyrazole), J_{H-H} = 5 Hz); 6.97 (m, 4H, CH (phenyl), J_{H-H} = 5 Hz); 6.31 (t, 2H, CH (4, pyrazole), J_{H-H} = 5 Hz); 5.99 (s, 4H, CH_2), **^{13}C NMR(DMSO, 500MHz) δ ppm:** 167.79 (C–N); 139.68 (CH (3, phenyl)); 138.99 (C–OH); 130.48 (CH (5, phenyl)); 129.32 (CH (5, pyrazole)); 110.42 (CH (3, pyrazole)); 105.91 (CH (4, pyrazole)); 59.09 (CH_2).

- **5-bromo-N-((3,5-dimethyl-1H-pyrazol-1-yl) methyl) pyridin-2-amine(6):** For this preparation, 1g of 3-amino-4-bromopyridine (5.8 mmol) and 1.46g of (3,5-dimethyl-1H-pyrazol-1-yl)methanol (11.6 mmol) were mixed together in acetonitrileunder reflux for 4 h, and the solvent was evaporated then recrystallized in diethyl ether then filtrated to have the final product (1.72 g, 76%);**FTIR(KBr, cm^{-1}):** 3040 (C–H); 1558 (C=C); 1542 (C–C); 1320 (C–N); 1170 (C=N); 1030 (N–N); 742 (=C–H); 680 (C–S), **^{1}H NMR(DMSO, 400MHz) δ ppm:** 7.57 (d, 1H, CH–N (Pyridine), J_{H-H} = 5 Hz); 6.90 (d, 2H, CH=CH (Pyridine), J_{H-H} = 5 Hz); 6.12 (s, 1H, CH (4, Pyrazole)); 5.76 (t, NH, J_{H-H} = 5 Hz); 5.59 (d, 4H, CH_2, J_{H-H} = 5 Hz); 2.5 (s, 3H, CH_3 (5, pyrazole)); 2.16 (s, 3H, CH_3 (3, pyrazole)), **^{13}C NMR(DMSO, 400MHz) δ ppm:** 153.64 (C–N); 146.94 (C–CH_3 (3, pyridine)); 140.15 (C–CH_3 (5, pyridine)); 133.32 (CH–N (Pyridine)); 113.53 (CH=CH (Pyridine)); 105.79 (CH (4, Pyrazole)); 61.32 (CH_2); 13.83 (CH_3 (3, pyrazole)); 10.29 (CH_3 (5, pyrazole)).

2.3. DFT calculations

The DFT study was executed on Dell OptiPlex 790 MT - Core i5-2400 @ 3,10 GHZ with 4 GB RAM PC-based - Windows 7 Pro 64 Bits as operating system. Full geometry optimization of the studied molecules have been performed using **Gaussian 09W software** (Frisch et al., 2009) by the Density Functional Theory (DFT) method with the 3 functional parameters of Becke associated with the functional correlation gradient corrected of Lee Yang Parr (B3LYP) exchange correlation (Becke, 2014; Becke and Becke, 1993; Lee et al., 1988) in combination with 6-31G (d, p) orbital basis sets for all atoms. No symmetry constrains was applied during the geometry optimization. Molecular Electrostatic Potential (MEP) maps of the optimized structures were calculated and generated by GaussView 06 software.

2.4. Molecular docking

The crystal structure of the Urate oxidase (PDB: 1R4U) (Retailleau et al., 2004) was downloaded from Protein Database Bank (www.rcsb.org) then used as a biological target in the docking study. The sequence of the protein was edited by removing water molecules and cofactors using default parameters included in **MOE software**. The active site was searched using the site finder tool. The docking was launched after protonating the protein at pH = 7 and adding partial charges. The complex was optimized under MMFF94X forcefield. Protein was kept in a rigid conformation while ligands in flexible conformation.

2.5. Antioxidant activity

DPPH ((1,1-diphenyl-2-picrylhydrazyl) assay was used in this work to evaluate the antioxidant potential of all the prepared compounds (Cuvelier and Berset, 1995). Briefly, 2 mg of DPPH was dissolved in 100 mL of Methanol to obtain the solution (**M**). On the other side, the concentration ranging from 2 to 500 µg/mL of both ligands and ascorbic acid (positive control) was prepared. For our tests, 0.5mL of (**M**) was mixed with 0.5 mL of each ligand, then incubated in the dark for 30 min, the

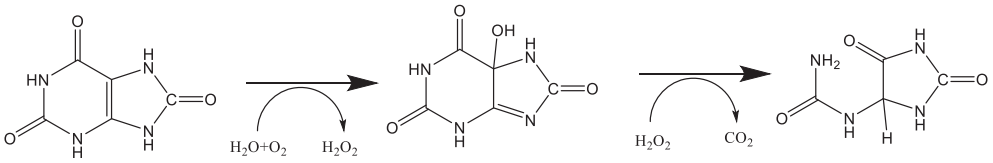

Figure 6. The schematic degradation of uric acid to (5-hydroxyisourate) then allantoin (Retailleau et al., 2004).

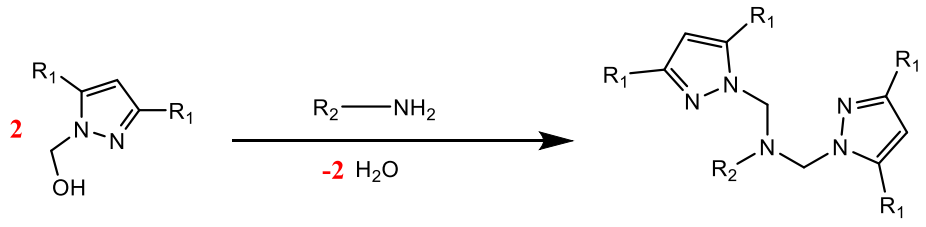

Figure 7. The general procedure for the preparation of the ligands 1-6.

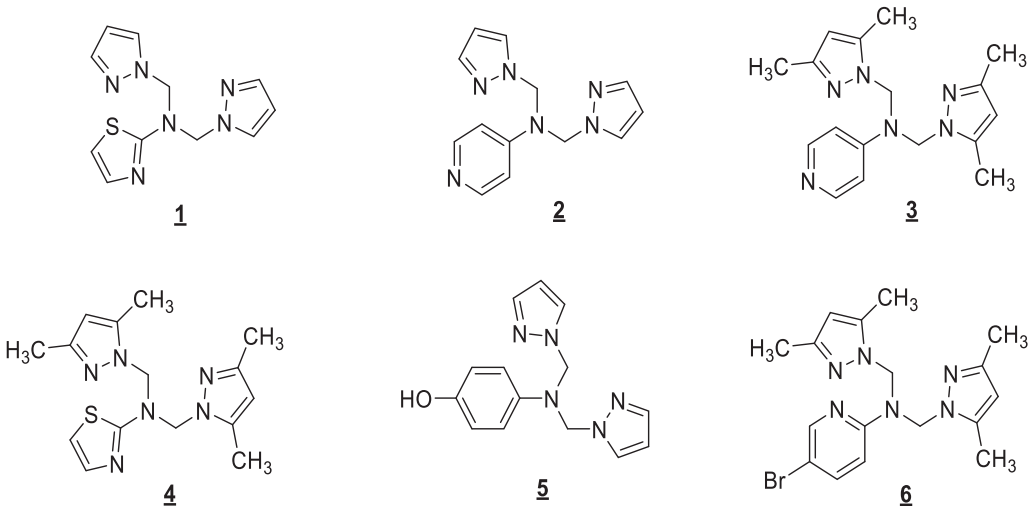

Figure 8. The chemical structures of the prepared ligands 1-6.

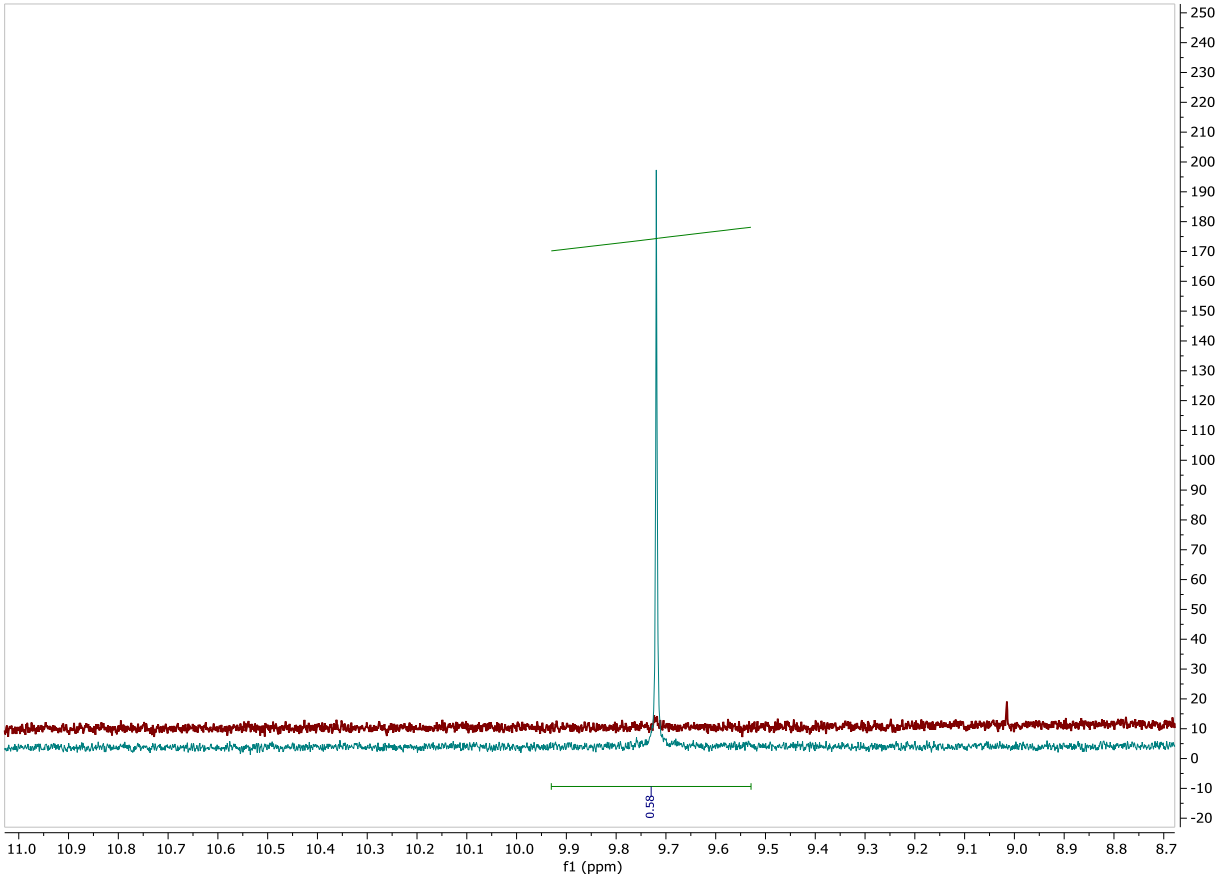

Figure 9. OH region representation in 1H NMR spectrum of the ligand (1) (Red) superposed with the spectrum of Pyrazol-1-yl-methanol (Blue).

absorbance of each mixture was measured with the aid of a UV spectrophotometer at 517 nm.

However, the activity is defined by the percentage of the scavenging activity calculated using the following equation:

$$\%scavenging\ activity = (A_{control} - A_{Sample} / A_{control}) \times 100 \quad (1)$$

Where $A_{control}$ is the absorbance of the blank (DPPH alone) and A_{Sample}: the absorbance of the tested solution after t = 30 min.

3. Results and discussion

3.1. Chemistry

A library of tridentate pyrazolic compounds 1–6 was prepared according to (Figures 7 and 8) by condensation of the (3,5-dimethyl-1H-pyrazol-1-yl) methanol ($R_1 = CH_3$) and the Pyrazol-1-yl-methanol ($R_1 = H$) (Dvoretzky and Richter, 1950) with appropriate primary amines under reflux in acetonitrile for 4 h by following the literature procedure

(Abrigach et al., 2014a,b; Kaddouri et al., 2017; Oussaid et al., 2014; Rachid et al., 2009).

The chemical structure of the studied ligands was verified by the absence of OH in the ligand spectrum, as an example: NMR spectrum superposition of the ligand 1 with Pyrazol-1-yl-methanolrepresented in Figure 9.

3.2. Antioxidant activity (DPPH assay)

Table 1 which represent the IC_{50} values of each studied ligand either in μg/ml and μM, show us the IC_{50} of the different ligands where we see that the ligand (**4**) has the best IC_{50} value with 4.67 μg/mL compared to the IC_{50} of the Ascorbic acid which is 2 μg/mL.

The ligand **4** has no Proton to give to DPPH radical, but it is rich in electron, and we proposed due it structure that it gives electron to stabilize the DPPH radical; by the delocalization of the electron over the molecule so it doesn't dimerize, as the most other free radicals (Molyneux, 2004). For the stabilization of free radicals, in our case the DPPH are either by Proton or electron donation (Güder, 2016; Molyneux, 2004), or called as redox based reaction (ET: Electron Transfer or HAT: Hydrogen atom transfer that react either with reactive oxygen species (ROS) or reactive nitrogen species (RNS) (Li et al., 2018). This pushes us to do theoretical investigations to have more insights about the molecular reactivity of our studied ligands (1–6).

3.3. Theoretical investigations

3.3.1. DFT calculations

The determination of the electronic parameters of a molecule is an efficient tool to predict and interpret its reactivity in several types of reactions and remains a powerful technique to explain the biological activity results (Demir et al., 2016; Karrouchi et al., 2017). The frontier molecular orbital HOMO (The highest occupied molecular orbital) and LUMO (The lowest unoccupied molecular orbital) present important descriptors that can use it to determine the electron donating and receiving ability of a molecule. Additionally, the energy gap ($\Delta E = E_{LUMO} - E_{HOMO}$) is a very established indicator of the chemical reactivity and stability, it is a measure of the intramolecular charge transfer. Generally, molecules with a large energy gap are associated with less chemical reactivity and high kinetic stability, and vice versa for molecules with a small energy gap (Lamsayah et al., 2016). In our case, these parameters were calculated for the most active antioxidant compound (compound **4**) and the less active one (compound **2**) after full-geometry optimization at DFT/B3LYP/6-31G (d,p) level. The shapes of MOs frontiers HOMO and LUMO and their energy values were determined and displayed in the Figure 10.

From the DFT results, LUMO energies of **2** and **4** were found in order of -0.552 and -0.016eV respectively. HOMO energies were -6.260 eV for compound **2** and -5.523 eV for compound **4**, leading to energy gap values of 5.707 and 5.507 eV for **2** and **4** respectively, which means that

Table 1. The IC_{50} antioxidant activity results of synthesized compounds (**1**-**6**) and the Ascorbic acid reference.

Compound		**1**	**2**	**3**	**4**	**5**	**6**	Ascorbic acid
IC_{50}	μg/mL	20.56	45.32	33.78	**4.67**	15.46	26.05	2
	μM	78.98	178.21	108.82	**14.76**	57.41	66.91	11.36

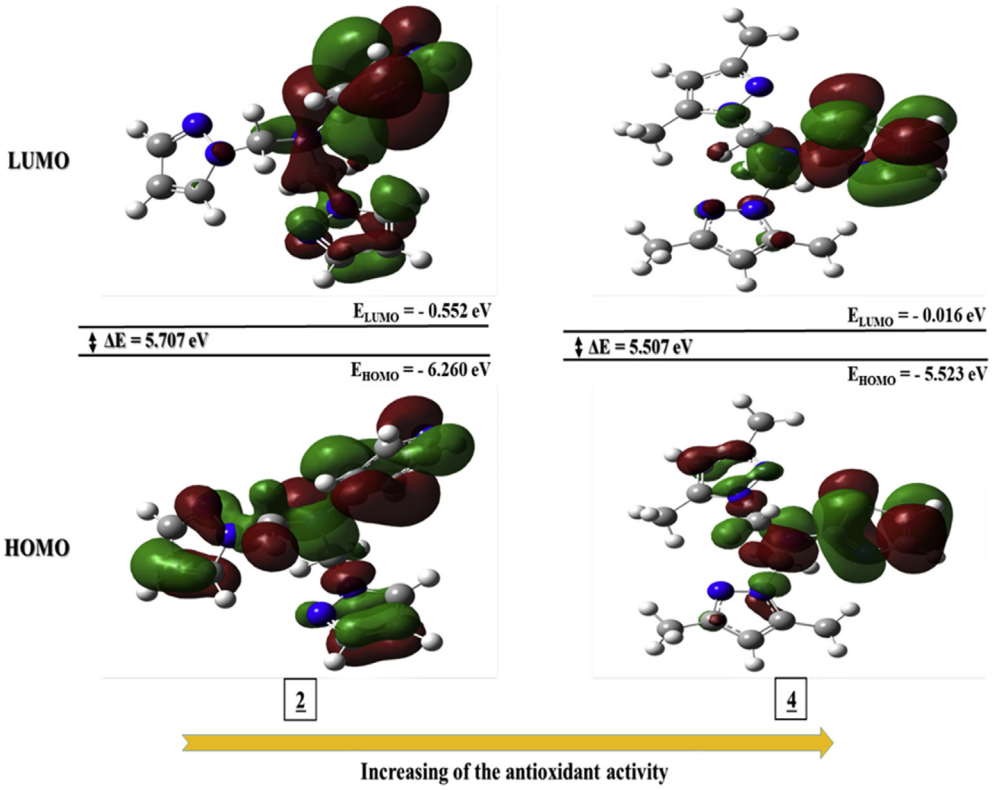

Figure 10. Shapes of HOMO, LUMO of compounds **2** and **4** in correlation with the antioxidant activity. Positive and negative phases are shown in red and green colors, respectively.

Table 2. The calculated molecular descriptors of compounds 2 and 4.

Chemical reactivity indices (eV)	2	4
E_{HOMO}	- 6.260	-5.523
E_{LUMO}	- 0.552	- 0.016
$\Delta E = E_{LUMO} - E_{HOMO}$	5.707	5.507
Chemical hardness ($\eta = (E_{LUMO} - E_{HOMO})/2$)	2.853	2.753
Softness ($\sigma = 1/\eta$)	0.350	0.363

Table 3. The docking calculations of compounds 2 and 4.

Compound	$\Delta G_{binding}$ (kcal/mol)	Interaction(C-AA)	Bond length (Å)
2	-4.96	N(pyridine) – H(Val227)	2.70
		Pyridine ring – H(Arg176)	3.87
4	-5.45	N(pyrazole) – H(Arg176)	2.39
		Pyrazole ring – H(Leu170)	2.98
		$H(CH_3)$ – Phenyl (Phe159)	3.04
		Pyrazole ring – H(His256)	3.43

C-AA: Interaction between the studied compound and the Amino acid of the Xanthine oxidoreductase sequence.

compound 4 is less stable (therefore more active) than compound 2 because it opposes less charge transfer and changes in its electron density. In conclusion, these findings agree with our experimental results. The general shape of the molecular orbital and its location also represents an additional factor that can affect the biological activity of a molecule. It can be affected easily by the presence (or not) of electron-donating or withdrawing groups.

From the Figure 10, the HOMOs are delocalized over the entire molecule for compound 2, and mainly localized over thiazole ring, sp^3-nitrogen atom of the bridge bond and on one of pyrazolerings for compound 4. The empty LUMO orbital is located on the pyridine ring, sp^3-nitrogen atom of the bridge bond and one of the pyrazole moieties, while it has its major contribution from thiazole ring, and sp^3-nitrogen atom of the bridge bond for compound 4.

On the other hand, several other chemical descriptors such as chemical hardness (η) and softness (σ) can also present a way to measure the reactivity of molecules (Tighadouini et al., 2019). Their values are generally calculated from the HOMO and LUMO energies. The results are collected in the Table 2 below. Compound 2 showed a chemical hardness value of 2.853 eV higher than that of compound 4 (2.753 eV) which

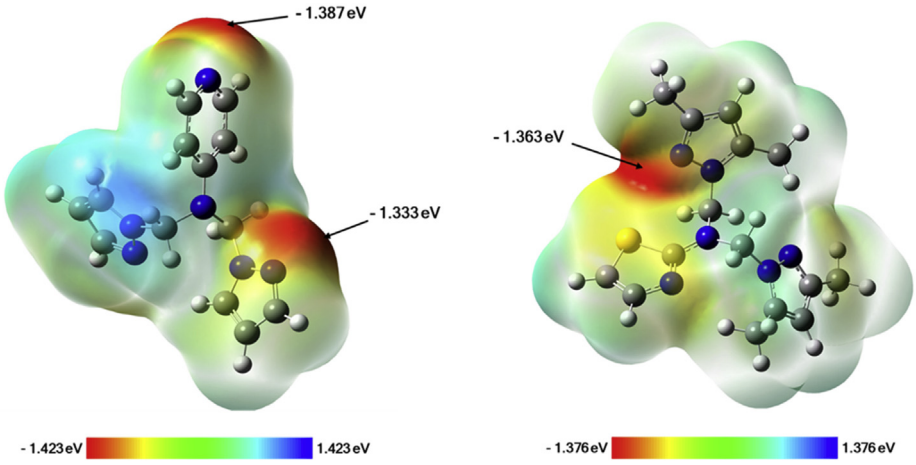

Figure 11. Molecular electrostatic potential (MEP) maps of compound 2 (left) and compound 4 (right). Negative regions are represented by red, orange and yellow colors, whilepositive regions are illustrated by green and blue colors. The electrostatic potential at the surface increases in the order red < orange < yellow < green < blue.

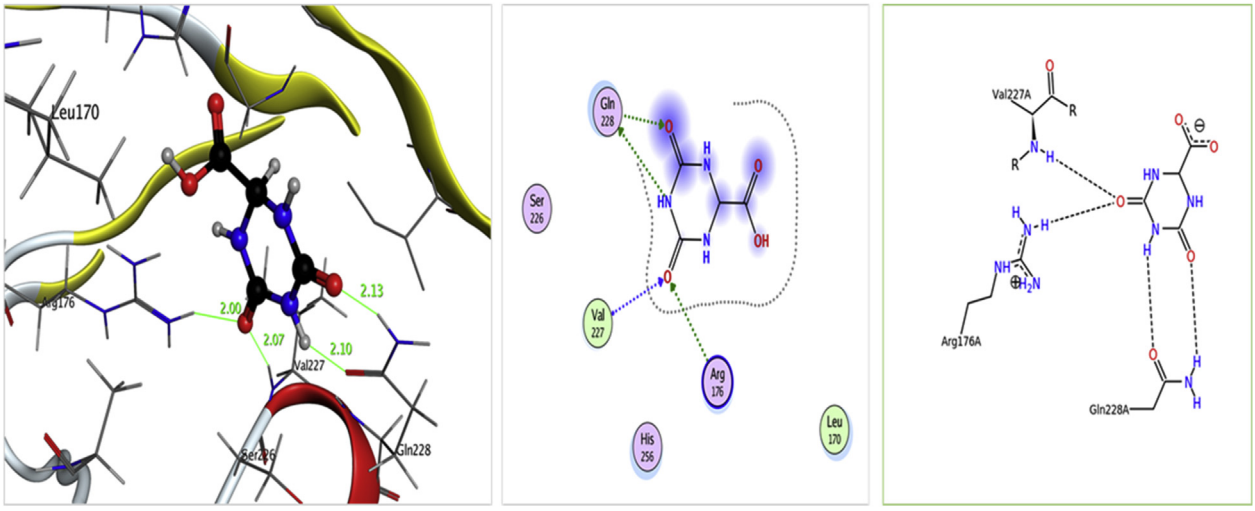

Figure 12. 3D (left) and 2D (middle) interactions of native ligand (oxonic acid) after re-docking protocol. Most-right figure represents the experimental interactions of the native ligand.

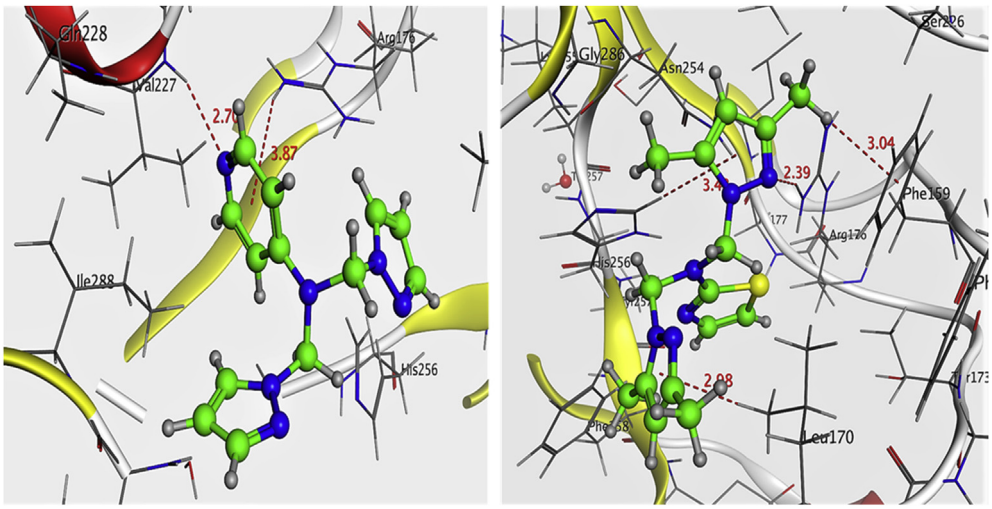

Figure 13. 3D binding modes of compound **2** (left), compound **4** (right) into the xanthine oxidoreductase binding pocket.

means that this compound resists more towards the deformation of the electron density distribution, hence more stable and less reactive compared to **4**. In general, high chemical hardness values characterize stable, hence low reactive compounds, whilst high values of softness, denote low stable compounds with high reactivity. All these observations were found to support the experimental antioxidant findings.

Finally, in order to determine the distribution of the electronic charge over all the structure, a molecular electrostatic potential (MEP) map was generated for each studied compound (i.e. **2** and **4**). In fact, MEP plot is very utilized as a powerful tool to identify the reactive sites for nucleophilic and electrophilic attacks on a molecule, to study the hydrogen bonding interactions and as well as the biological recognition processes (Pillai et al., 2017). Analyzing the created MEP maps for both compounds **2** and **4** (Figure 11), the highly negative electrostatic potential regions (red color) are mainly concentered over the nitrogen atoms of the pyridine and the pyrazole rings for compound **2** with values of- 1.387 and -1.333eV (at an isovalue of 0.0004 electrons/Å^3) respectively, in time the highly positive regions (blue color) are localized on the nitrogen atom of the second pyrazole ring. For compound **4**, the negative values are mainly located over the nitrogen atom of pyrazole ring with a value of -1.363 eV (low values were recorded over the nitrogen and sulfur atoms of the thiazole ring (yellow color)), while the plot showed low positive values focused mainly over the methyl groups (green color). These findings can be used to predict the possible sites for electrophilic attacks, a thing that can explain the docking results mentioned below with regard to the binding of each molecule to the residues of the active site of the studied protein.

3.3.2. Molecular docking

In order to understand and identify the molecular interactions between the ligand and the active site residues of the studied target protein; molecular docking was conducted employing Molecular Operating Environment (MOE) software. Crystal structure of the Urate oxidase (PDB entry 1R4U) was used in this study. The calculations were carried out keeping the default parameters of the MOE program.

As a first step, the docking reliability was checked by re-docking the native ligand (oxonic acid) into the binding site of Urate oxidase protein. The docking calculation showed that the predicted pose of re-docked ligand was found to be identical to that of the native ligand with rmsd = 0.970 Å (Figure 12) with a binding score of -4.45 kcal/mol. Predicted pose showed H-bonding interactions with amino acid residues Gln228, Val227 and Arg176 which is in total agreement with that shown in the experimental part.

In our present work, and based on the in vitro antioxidant assay findings, the two compounds **2** and **4**, which present the less and the most active compounds respectively, were docked into the active site of Urate oxidase protein. The molecular docking data are calculated and reported in Table 3.

According to the docking results, compound **4** showed a binding affinity to Urate oxidase protein higher than shown by compound **2**, the values are equal to-5.45 and -4.96 kcal/mol for **4** and **2** respectively. As shown in Table 3 and depicted in Figure 13, both ligands interact with amino acid residues of Urate oxidase. Compound **2** was found to establish one hydrogen bonding interaction of 2.70 Å with amino acid residue Val227 and via the nitrogen atom of the pyridine ring and one π interaction between the pyridine ring and the hydrogen atom of NH_2 group of the Arg176 residue with a distance of 3.87Å. While, compound **4** form four interactions divided on one H-bond and three π interactions, the first was formed between the sp^{2}nitrogen atom of pyrazole ring and the hydrogen atom of Arg176 residue (2.39Å); two of the π interactions were made between the two pyrazole rings and the Leu170 and His256 residues with Bond length of 2.98 and 3.43 Å respectively; whilst the CH_3group via its hydrogen atom form the third one with the phenyl ring of Phe159 amino acid (3.04Å). Interestingly, compound **2** showed interactions with the same amino acids that interact with the native ligand, Val227 and Arg176, which can indicate that this compound can exhibit its action with a similar mechanism like that of the native ligand.

Based on the above observations, our docking results revealed that the compound **4** seems more active than **2**, which support the experimental antioxidant findings. However, more appropriate experimental tests should and more theoretical investigations by others performing methods should be carried out to confirm the effect of these compounds on Urate oxidase protein.

4. Conclusion

Six ligands were prepared by condensation of 1,3-Thiazole or Pyridine derivatives with 1H-pyrazole or 3,5-dimethylpyrazole to give good yields up to 99%. From the DFT results, compound **4** is less stable (therefore more active) than compound **2**. Compound **2** showed a chemical hardness value of 2.853 eV higher than that of compound **4** (2.753 eV) which means that this compound resists more towards the deformation of the electron density distribution, hence more stable and less reactive compared to **4**. In general, high chemical hardness values characterize stable, hence low reactive compounds, whilst high values of softness, denote low stable compounds with high reactivity. All these results support our experimental findings. Based on the above observations, our docking results revealed that compound **4** seems more active than **2**, which is in good accordance with the experimental antioxidant findings. However, more experimental tests and theoretical

investigations should be carried out by other performing methods to confirm the effect of these compounds on Urate oxidase protein.

Declarations

Author contribution statement

Y. Kaddouri: Conceived and designed the experiments; Performed the experiments; Analyzed and interpreted the data; Wrote the paper.

E Youssfi: Performed the experiments.

Farid Abrigach: Analyzed and interpreted the data; Wrote the paper.

Mohamed El Kodadi: Analyzed and interpreted the data.

R. Touzani: Contributed reagents, materials, analysis tools or data; Wrote the paper.

Funding statement

This research did not receive any specific grant from funding agencies in the public, commercial, or not-for-profit sectors.

Competing interest statement

The authors declare no conflict of interest.

Additional information

No additional information is available for this paper.

References

Abdel-sattar, N.E.A., El-naggar, A.M., 2017. Novel Thiazole Derivatives of Medicinal Potential: Synthesis and Modeling, 2017(d).

Abrigach, F., Khoutoul, M., Merghache, S., Oussaid, A., Lamsayah, M., Zarrouk, A., et al., 2014a. Antioxidant Activities of N-((3,5-dimethyl-1H-pyrazol-1-yl) methyl) pyridin-4-amine derivatives. Der Pharma Chem. 6 (3), 280–285.

Abrigach, F., Khoutoul, M., Benchat, N., Radi, S., Draoui, N., Riant, O., Touzani, R., 2014b. Library of synthetic compounds based on pyrazole unit: design and screening against breast and colorectal cancer. Lett. Drug Des. Discov. 3 (3), 1010–1016.

Becke, A.D., 2014. A new mixing of Hartree–Fock and local density-functional theories. J. Chem. Phys. 1372(1993).

Becke, A.D., Becke, A.D., 1993. Density Functional Thermochemistry. III. The Role of Exact Exchange Density-Functional Thermochemistry. III. The Role of Exact Exchange, 5648.

Carolina, N., 2008. Pyridines and Their Benzo Derivatives: Reactivity at the Ring.

Chauhan, A., Sharma, P.K., Kaushik, N., 2011. Pyrazole: a versatile moiety. Int. J. Chem. Res. 3 (1), 11–17.

Cuvelier, M.E., Berset, C., 1995. Use of a Free Radical Method to Evaluate Antioxidant Activity. LWT - Food Sci. Technol. 30, 25–30.

Demir, S., Tinmaz, F., Dege, N., Ilhan, I.O., 2016. Vibrational spectroscopic studies, NMR, HOMO-LUMO, NLO and NBO analysis of 1-(2-nitrobenzoyl)-3,5-diphenyl-4,5-dihydro-1H-pyrazole with use X-ray diffractions and DFT calculations. J. Mol. Struct. 1108, 637–648.

Dvoretzky, I., Richter, G.H., 1950. Formaldehyde condensation in the pyrazole series. J. Org. Chem. 15 (6), 1285–1288.

Farbstein, D., Kozak-Blickstein, A., Levy, A.P., 2010. Antioxidant vitamins and their use in preventing cardiovascular disease. Molecules 15 (11), 8098–8110.

Frisch, M.J., Trucks, G.W., Schlegel, H.B., Scuseria, G.E., Robb, M.A., Cheeseman, J.R., et al., 2009. Gaussian 09, Revision A.02. Gaussian, Inc., Wallingford CT.

Güder, A., 2016. Influence of total anthocyanins from bitter melon (Momordica charantia Linn.) as antidiabetic and radical scavenging agents. Iran. J. Pharm. Res. (IJPR): IJPR 15 (1), 301–309.

Hussein, W., Turan, G., 2018. Synthesis of new thiazole and thiazolyl derivatives of medicinal significant-a short review. MOJ Biorg. Org. Chem. 2 (2), 52–55.

Kaddouri, Y., Takfaoui, A., Abrigach, F., El Azzouzi, M., Zarrouk, A., El-Hajjaji, F., et al., 2017. Tridentate pyrazole ligands: synthesis, characterization and corrosion inhibition properties with theoretical investigations. J. Mater. Environ. Sci. 8 (3), 845–856.

Kalanithi, M., Rajarajan, M., Tharmaraj, P., Johnson Raja, S., 2015. Synthesis, spectroscopic characterization, analgesic, and antimicrobial activities of Co (II), Ni (II), and Cu (II) complexes of 2- [N, N-bis-(3,5-dimethyl-pyrazolyl-1- methyl)] aminothiazole. Med. Chem. Res. 24 (4), 1578–1585.

Karrouchi, K., Radi, S., Ramli, Y., Taoufik, J., Mabkhot, Y.N., 2018. Synthesis and pharmacological activities of pyrazole derivatives: a review. Molecules 23.

Karrouchi, K., Yousfi, E.B., Sebbar, N.K., Ramli, Y., Taoufik, J., Ouzidan, Y., et al., 2017. New pyrazole-hydrazone derivatives: X-ray analysis, molecular structure investigation via density functional theory (DFT) and their high in-situ catecholase activity. Int. J. Mol. Sci. 18, 1–14.

Khan, M.F., Alam, M.M., Verma, G., Akhtar, W., Akhter, M., Shaquiquzzaman, M., 2016. The therapeutic voyage of pyrazole and its analogs: a review. Eur. J. Med. Chem. 120, 170–201.

Lamsayah, M., Khoutoul, M., Takfaoui, A., Touzani, R., 2016. High liquid – liquid extraction selectivity of Fe (II) and Pb (II) with TD-DFT theoretical calculations of long chain acid pyrazole- and triazole-based ligands. Cogent Chem. 1–16.

Lee, C., Hill, C., Carolina, N., 1988. Development of the Colle-Salvetti correlation-energy formula into a functional of the electron density. Phys. Rev. B 37 (2).

Lettre, D.P., Gaware, V.M., Dighe, N.S., Pattan, S.R., Shinde, H.V., 2010. Scholars Research Library, 2, pp. 35–40.

Li, X., Chen, B., Xie, H., He, Y., Zhong, D., Chen, D., 2018. Antioxidant structure–activity relationship analysis of five dihydrochalcones. Molecules 23 (5), 1–13.

Molyneux, P., 2004. The use of the stable free radical diphenylpicryl-hydrazyl (DPPH) for estimating antioxidant activity. Songklanakarin J. Sci. Technol. 26 (December 2003), 211–219.

Nayak, Swarnagowri, Gaonkar, S.L., 2019. A review on recent synthetic strategies and pharmacological importance of 1,3-thiazole derivatives. Mini Rev. Med. Chem. 19 (3), 215–238.

Oussaid, A., Touzani, R., Loupy, A., 2014. Evaluation of microwave effect on the selective dealkylation of alkyl aryl ether in solvent-free heterogeneous basic media. J. Mater. Environ. Sci. 5 (3), 739–746.

Pietta, P.G., 2000. Flavonoids as antioxidants. J. Nat. Prod. 63 (7), 1035–1042.

Pillai, R.R., Menon, V.V., Mary, Y.S., Armaković, S., Armaković, S.J., Panicker, C.Y., 2017. Vibrational spectroscopic investigations, molecular dynamic simulations and molecular docking studies of N'-diphenylmethylidene-5-methyl-1H-pyrazole-3-carbohydrazide. J. Mol. Struct. 1130, 208–222.

Process, R., Fujisawa, P.T.E., Patent, U.S., Seika, S., Co, C., Method, I., et al., 2002. Pyridine, pp. 2–6.

Rachid, T., Abdelkrim, R., Sghir, E.K., 2009. Synthesis and applications: ten years of experience in monodentate, bidentate, tridentate and macrocycle pyrazole heterocyclic chemistry. ChemInform 4 (13), 906–912.

Retailleau, P., Colloc'h, N., Vivarès, D., Bonneté, F., Castro, B., El Hajji, M., et al., 2004. Complexed and ligand-free high-resolution structures of Urate oxidase (Uox) from Aspergillus flavus: a reassignment of the active-site binding mode. Acta Crystallogr. Sect. D Biol. Crystallogr. 60 (3), 453–462.

Scarim, B., Jornada, D.H., Gabrielle, M., Machado, M., Maria, C., Ferreira, R., et al., 2019. Thiazole, thio and semicarbazone derivatives against tropical infective diseases: Chagas disease, human African trypanosomiasis (HAT), leishmaniasis, and malaria. Eur. J. Med. Chem. 162, 378–395.

Tareq, A.M., Farhad, S., Chakraborty, S., 2019. Experimental analysis of isolated compounds of Borreria hispida (L) in the context of antioxidant. Discovery Phytomedicine 6 (3), 138–142.

Tighadouini, S., Radi, S., Abrigach, F., Benabbes, R., Eddike, D., Tillard, M., 2019. Novel β-keto-enol pyrazolic compounds as potent antifungal agents. Design, synthesis, crystal structure, DFT, homology modeling, and docking studies. J. Chem. Inf. Model. 59.

Varghese, N., Jacob, J., Mythri, M., Nija, B., Sheeba, S.J.T., 2016. Synthesis of thiazole derivatives — a review. J. Pharm. Pharmacol. 5 (11), 624–636.

Yadav, P.S., Senthilkumar, G.P., 2011. Review article benzothiazole: different methods of synthesis and diverse biological activities. Int. J. Pharm. Sci. Drug Res. 3 (1), 1–7.

Yerragunta, V., Suman, D., Anusha, V., 2014. Pyrazole and its biological activity. PharmaTutor 2 (1), 40–48.